Power Oscillation Damping Improvement by Adding Multiple Wind Farms to Wide-Area Coordinating Controls

Andres E. Leon, *Member, IEEE*, and Jorge A. Solsona, *Senior Member, IEEE*

***Abstract*—This paper examines the feasibility of coordinating variable-speed wind farms with other power system devices, such as flexible ac transmission systems and synchronous generators, to damp low-frequency oscillations. For this purpose, an observer-based state-feedback approach is used to build a power oscillation damping (POD) controller, implemented through coordinated actions of multiple control devices, and able to manage several measurement channels. The wide-area POD controller also presents a time-delay compensation stage to mitigate adverse effects of latency involved in wide-area communication systems. Several practical issues are discussed and analyzed, such as measurement and control selection, model-order reduction, transmission time-delay compensation, impact of the POD control on wind farms, and robustness aspects. The control performance is evaluated and compared with other control schemes using eigenvalue analyses and nonlinear time-domain simulations over a wide range of operating conditions, for example, severe system faults, $N-1$ outage contingencies, load/generation shedding, and line tripping.**

***Index Terms*—Inter-area oscillations, phasor measurement unit (PMU), wide-area measurement systems (WAMS), wind energy conversion systems (WECS), wind power integration.**

I. Introduction

RENEWABLE energy penetration can impact on the power system stability. The system transient behavior can be deteriorated by reconfiguration of line power flows, reduction of system inertia, and interaction of converter controls with power system dynamics. On the other hand, the increasing power demand, slow transmission infrastructure expansion, and distance between renewable large power plants and load centers can also reduce the mode damping and push the system to its stability limits [1]. The aforementioned issues diminish the transmission capability and restrict the interconnection of large-scale systems due to low-frequency oscillations (LFOs) [2]. Classical power system stabilizer (PSS) approaches using local measurements can damp certain modes, but they lack sufficient observability to damp inter-area oscillations [3], [4]. In this context, power system operators are looking for solutions to enhance stability margins using modern available technologies and maximize the utilization of the existing facilities.

Variable-speed wind energy conversion systems (VS-WECS) are a mature technology which can accomplish several network support tasks such as voltage control, reactive power compensation, and short-term frequency regulation [5]–[7]. However, the ability of multiple VS-WECS to be coordinated with flexible ac transmission systems (FACTS) and synchronous generators (SGs) to damp LFO modes has not been thoroughly investigated. This ability can now be achieved by centralized coordination control, using the advances in wide-area measurement systems (WAMS).

Global positioning system (GPS)-synchronized phasor measurement technology allows phasor data concentrators (PDCs) to collect time-stamped data from many phasor measurement units (PMUs) and rebroadcast wide-area signals to control centers [8]. Time delays (or latency) involved in the whole wide-area communication system can reach several hundreds of milliseconds, and have to be considered in the control design stage to improve the controller performance [9]. Different solutions to compensate time delays in wide-area coordinating (WAC) controllers were proposed: Smith predictor [10], [11]; gain scheduling [12]; adaptive phase-shift algorithms [13]; model extension using Padé approximations [14]–[17]; and phase compensation with lead-lag filters [18].

The main approaches used to build centralized or WAC controllers can be classified into four categories: 1) residue-based methods [2], [18], [19]; 2) H_∞ control strategies [4], [11], [12], [20]; 3) control tuning based on optimization procedures [3], [16], [21]; and 4) state-space approaches, such as observer-based state-feedback control [22], [23], output-feedback linear-quadratic regulator (LQR) [17], [24], and linear-quadratic-Gaussian (LQG) control [14], [15], [25], [26]. Other control structures can also be mentioned such as feedback linearization [10], model predictive control [27], and fuzzy logic [28]. From the above works, the potential of WAC controllers to simultaneously coordinate SGs and FACTS was explored in [3], [10], [16], but they did not include wind farms in their studies. Photovoltaic and wind power plants have been recently used to damp power system oscillations by measuring local [29]–[31] or remote [15], [32], [33] signals. However,

Manuscript received June 07, 2013; revised October 05, 2013; accepted November 04, 2013. Date of publication November 22, 2013; date of current version April 16, 2014. This work was supported in part by Universidad Nacional del Sur, Consejo Nacional de Investigaciones Científicas y Técnicas (CONICET), and Agencia Nacional de Promoción Científica y Tecnológica (ANPCyT), Argentina. Paper no. TPWRS-00743-2013.

The authors are with Instituto de Investigaciones en Ingeniería Eléctrica (IIIE) "Alfredo Desages" (UNS-CONICET), Universidad Nacional del Sur (DIEC-UNS), Bahía Blanca 8000, Argentina (e-mail: aleon@ymail.com).

Color versions of one or more of the figures in this paper are available online at http://ieeexplore.ieee.org.

Digital Object Identifier 10.1109/TPWRS.2013.2289970

these proposals lack a WAC control of renewable energy plants with other system devices, and their controllers only consider one measurement and one control action, single-input single-output (SISO) approach. In [34], an attempt to coordinate multiple devices was addressed using a complex neural-network based scheme, but without considering either multiple wind farms or communication time-delay compensation. A multiple-device controller to improve the short-term frequency regulation was proposed in [35]; nevertheless, SG load angles are needed (signals not directly available in power stations), as well as a number of measurements equal to the reduced-model order (condition not ideal for large-scale power systems).

The main contribution of this work is the coordination of multiple wind farm controllers with FACTS and SGs to damp low-frequency oscillations and enhance the power system operation. This is addressed through a WAC control synthesized using an observer-based state-feedback approach. VS-WECS can achieve these sorts of tasks via active power modulation resorting to the kinetic energy stored in their rotating masses, using the fast action of power electronics and, independently, injecting reactive power [6], [36]. The wide-area power oscillation damping (POD) controller is implemented through coordinated control actions of multiple power system devices (VS-WECS, FACTS and SGs) and multiple measurement channels, multi-input multi-output (MIMO) approach.

Standard control systems measuring local signals are used in the different facilities affected by the WAC control. Then, the WAC controller uses global or remote information to add supplementary damping signals to the local controllers. This two-layer or hierarchical approach [2]–[4], [17], [18] allows local controls to remain operational, in case the centralized control is turned off due to loss of PMU data or communication link failure, and be capable of guaranteeing an acceptable system performance.

The electrical network is continuously subject to several operating points due to system changes such as $N-1$ outage contingencies, generation and load shedding, and line tripping [14], [21]. For this reason, we also accomplish a robustness assessment of the proposed POD controller, including several system contingencies to show the satisfactory damping performance over a wide range of operating points.

This paper is organized as follows. Section II introduces the model of the power system case study. Measurement and control selections are discussed in Section III. Section IV describes the WAC control design. In Section V, eigenvalue analyses and nonlinear time-domain simulations are presented to assess and validate the controller performance. Finally, conclusions are given in Section VI.

II. Power System Case Study

The IEEE 50-machine 145-bus test system is used in this study (Fig. 1). To perform the study of coordinating conventional generators with new WECS and FACTS, we modified the original system to include 13 wind farms and two high-voltage direct-current (HVDC) transmission lines. Synchronous generators are represented by a fourth-order two-axis model equipped with automatic voltage regulator (AVR) type IEEE-ST1A, PSS type IEEE-PSS1A, and a third-order turbine-governor model [37]. The WAC control is performed in synchronous generators by adding a supplementary remote signal v_{cc} at the same place that the PSS output signal enters the excitation system [17], [18].

Wind power plants are represented by aggregated models [29], [38] based on variable-speed full-converter wind turbines. A two-lumped-mass model represents the wind turbine drive-train system [39]. The electrical machine consists of a permanent magnet generator, the parameters of which are taken from the Siemens wind turbine STW-3.0-101. An average model of voltage-source converters (VSCs) is considered for WECS and FACTS converters [40].

In the WECS controller, the active power reference p_w^{ref} consists of three terms: a term from the maximum power point tracking (MPPT) algorithm, a frequency regulation contribution based on a local frequency measurement [6], and a remote signal Δp_w from the WAC control. The reference of the reactive current is calculated from a grid code curve which relates the injection of reactive current with the voltage amplitude at the point of common coupling (PCC) [41]. A schematic block diagram of the WECS controller is shown in Fig. 2. Further details of WECS models and internal controllers can be found in [38], [40], and [42]. In shunt FACTS performing ac voltage regulation, like static synchronous compensators (STATCOMs) and VSC-HVDC stations, a conventional droop control is chosen to set their voltage/reactive current characteristic, plus an additional reactive power term Δq_f from the WAC control. FACTS and VSC-HVDC stations present similar control capabilities from the proposed control point of view; therefore, to reduce the notation, we consider both technologies as the same kind of control device.

III. Measurement and Control Selection

There are several techniques to select the best measurement and control signals: the residue approach [16], [20]–[23], modal and geometric measures of controllability and observability [2], [4], [11], [14], [15], participation factors [18], [43], singular value decomposition (SVD)-based index [3], relative gain array (RGA) [19], and combined residue/RGA methods [44], [45], among others [46].

Table I shows the most poorly damped modes of the system. All modes have a damping ratio higher than 5%, except the inter-area mode #1, which is the critical mode. Because bus voltage angles from PMUs have a high electromechanical mode observability, they were selected as candidate measurements [13], [22], [23]. The geometric measure technique was chosen to select the best signals to be fed back. The details of this approach, along with expressions to compute the observability and controllability indices, are given in [4]. We analyzed all voltage angle differences between each bus in the system. The voltage angle differences with the highest observability index were chosen to build the measurement vector of the WAC controller (first elements of the last column in Table I). In our case study, we found that using six measurements from the rows of the most poorly damped modes, a high damping performance

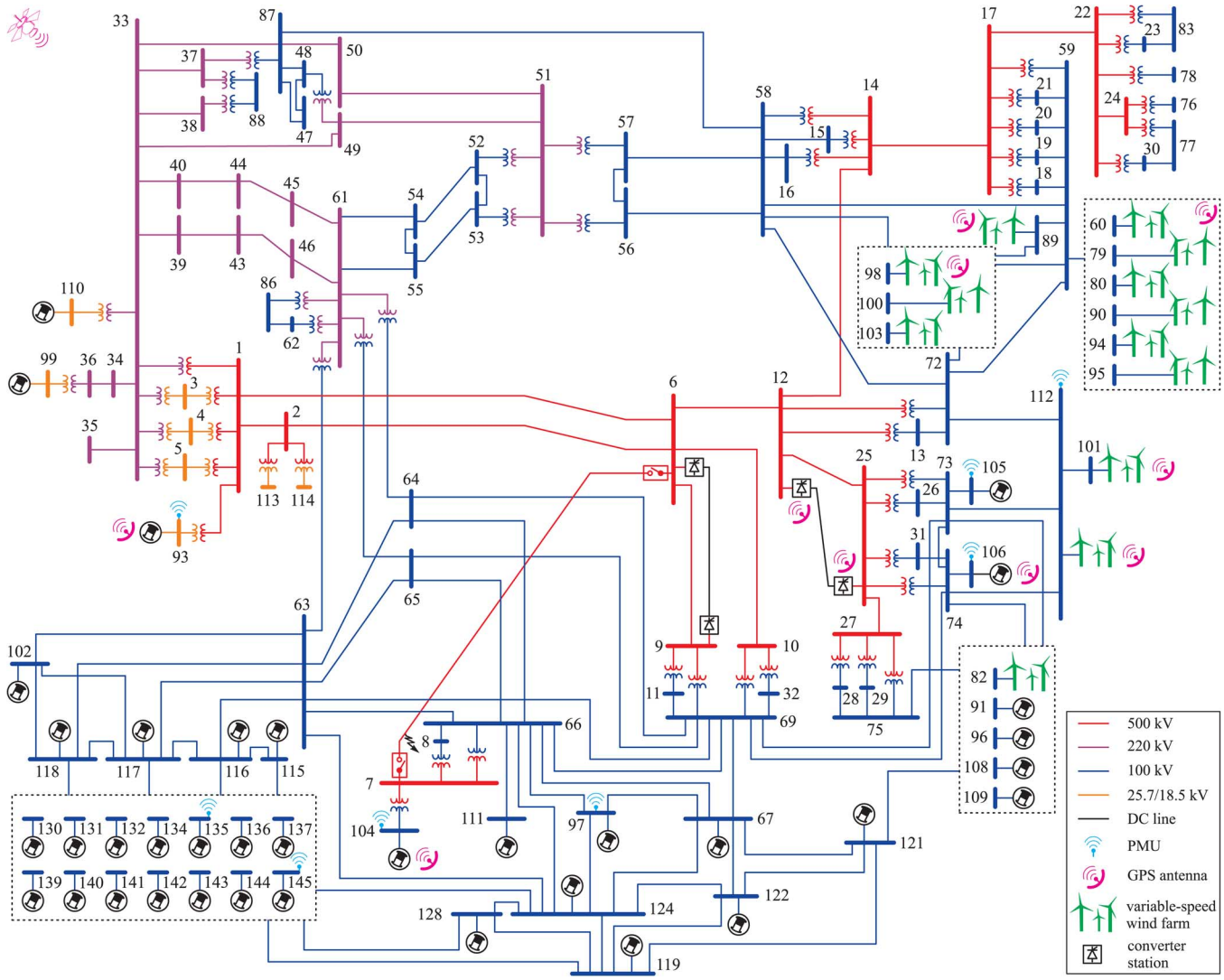

Fig. 1. Single-line diagram of the studied system, based on the IEEE 50-machine 145-bus test system.

is accomplished; accordingly, the measurement vector is set as follows:

$$\mathbf{y} = [(\theta_{93} - \theta_{145})\ (\theta_{93} - \theta_{97})\ (\theta_{106} - \theta_{97})\ (\theta_{135} - \theta_{112}) \\ (\theta_{105} - \theta_{106})\ (\theta_{104} - \theta_{106})]^T .$$

The measurement vector $\mathbf{y}$ determines the buses where PMUs must be placed (see Fig. 1). In the same way as the optimal measurements were obtained, we also calculated the best control inputs using the input signals with higher controllability index of the modes of interest. Both active and reactive powers of all VSC-HVDC links and FACTS devices can be included in the candidate set of control inputs; here, to simplify the amount of potential control signals, in VSC-HVDC stations only reactive powers were chosen as candidates for the WAC control.

Two cases were considered to analyze the possible improvements of including wind farm converters to wide-area POD controllers: the first one coordinates three SGs (#93, #104, #106) and the converter stations (#12, #25) of a HVDC line, and the second one, besides the SGs and HVDC stations, also includes

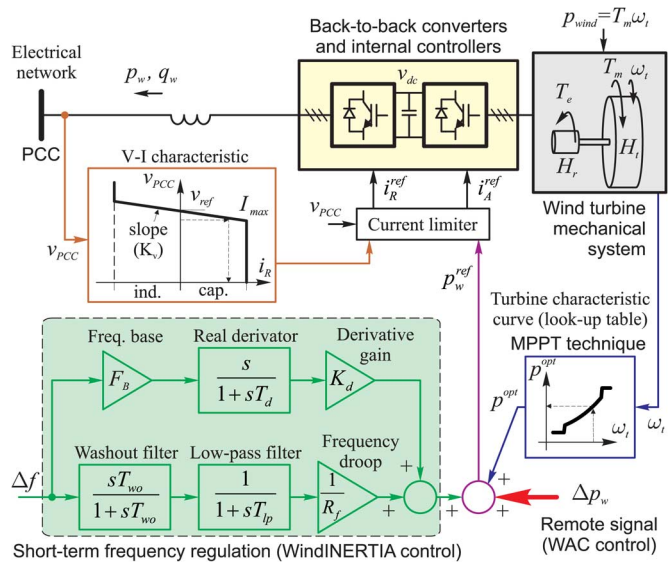

Fig. 2. Schematic block diagram of the WECS controller.

TABLE I
MODAL ANALYSIS

Mode number	f_n (Hz)	ζ (%)	Mode shape	Measurements with the highest modal observability (index × 100)
Mode #1	0.451	0.9	South area vs North area	θ_{93}-θ_{145}(4.3), θ_{99}-θ_{145}(4.0), θ_{110}-θ_{145}(4.0), θ_{112}-θ_{145}(3.9), θ_{93}-θ_{119}(3.9)
Mode #2	0.914	8.3	SG#93,#99,#110 vs System	θ_{93}-θ_{97}(6.4), θ_{110}-θ_{97}(6.4), θ_{110}-θ_{112}(6.4), θ_{110}-θ_{101}(6.4), θ_{99}-θ_{97}(6.3)
Mode #3	1.046	9.0	SG#105,#106 vs South area	θ_{106}-θ_{97}(2.9), θ_{105}-θ_{97}(2.6), θ_{106}-θ_{67}(2.5), θ_{105}-θ_{67}(2.3), θ_{106}-θ_{122}(2.3)
Mode #4	1.078	9.2	SG#135 vs System	θ_{135}-θ_{112}(8.6), θ_{135}-θ_{91}(8.6), θ_{135}-θ_{82}(8.6), θ_{135}-θ_{101}(8.6), θ_{135}-θ_{145}(8.6)
Mode #5	1.194	5.8	SG#105 vs SG#106	θ_{105}-θ_{106}(9.4), θ_{106}-θ_{26}(8.1), θ_{106}-θ_{73}(8.0), θ_{106}-θ_{112}(7.5), θ_{106}-θ_{101}(7.5)
Mode #6	1.364	7.9	SG#104,#111 vs System	θ_{104}-θ_{106}(1.8), θ_{104}-θ_{82}(1.8), θ_{104}-θ_{105}(1.7), θ_{104}-θ_{112}(1.7), θ_{104}-θ_{101}(1.7)
Mode #7	1.799	9.2	SG#104 vs SG#111	θ_{104}-θ_{111}(1.9), θ_{104}-θ_{8}(1.3), θ_{104}-θ_{66}(1.3), θ_{111}-θ_{7}(1.1), θ_{104}-θ_{67}(1.0)

five wind farms (#79, #89, #98, #101, #112) in the WAC control. Therefore, in the first case, called (conventional) C-WAC case, the control input is given by

$$\mathbf{u}_1 = [v_{cc93}\ v_{cc104}\ v_{cc106}\ \Delta q_{f12}\ \Delta q_{f25}]^T$$

and, in the second controller, called (wind farm) WF-WAC case, the control input is

$$\mathbf{u}_2 = [v_{cc93}\ v_{cc104}\ v_{cc106}\ \Delta q_{f12}\ \Delta q_{f25}\ \Delta p_{w79}\ \Delta p_{w89}\ \Delta p_{w98}\ \Delta p_{w101}\ \Delta p_{w112}]^T.$$

IV. WAC CONTROLLER DESIGN

The design procedure of the wide-area POD control was developed in four stages. First, we obtained a reduced-order model of the power system. Second, the model was extended with a transmission time-delay block to enhance the WAC control performance against typical delays of communication channels. Third, a state-feedback control law was computed, based on an optimal quadratic technique. Finally, a state observer was designed to estimate the reduced-model states required in the state-feedback control law.

A. Power System Model for the Controller Design

Power systems have thousands of states; to design a controller with such a high order is neither practical nor necessary; therefore, reduced models are usually calculated in the frequency range of interest [4], [24]. There are two ways to obtain the reduced model of a large power system. First, if the data of the large-scale system is available, model reduction techniques can be applied to obtain a lower-order representation; second, system identification algorithms capable of estimating MIMO models from time-domain data can be used, for example, numerical algorithms for subspace state-space system identification (N4SID) [18], [22], [43]. Time-domain input/output data can be obtained either from actual field measurements (e.g., from PMUs), or from a simulation software (e.g. PSS/E and DIgSILENT PowerFactory, which usually transmission system operators (TSOs) employ to study large-scale power systems).

In our study, we considered the first approach; the IEEE 50-machine 145-bus benchmark system was reduced by the balanced model truncation via the Schur method [14], [16], [25]. The resulting state-space realization is written as

$$\dot{\mathbf{x}}_r = \mathbf{A}_r\mathbf{x}_r + \mathbf{B}_r\mathbf{u} \tag{1}$$

$$\mathbf{y} = \mathbf{C}_r\mathbf{x}_r. \tag{2}$$

Details of the reduction methodology can be found in [47]. The vector $\mathbf{x}_r$ represents the internal states of the reduced model, whereas matrices $\mathbf{A}_r, \mathbf{B}_r$, and $\mathbf{C}_r$ are the state, input, and output matrices obtained using the reduction technique. To avoid adverse interactions, the WAC control design should contemplate the dynamics of local controllers; therefore, they were included in the above system model. The output vector $\mathbf{y}$ represents the measurements, and $\mathbf{u}$ is the input vector containing all of the supplementary control inputs such as the signals added to the excitation system of SGs (v_{cc}), and additional active and reactive powers injected by WECS (Δp_w) and FACTS (Δq_f).

B. Transmission Time-Delay Compensation

A time-delay model (a third-order Padé approximation) was embedded in the controller design to compensate time delays associated with wide-area measurements. To counteract any amplitude and phase shift, the pre-filter model of the signal conditioning stage was also added. The pre-filter consists of washout and low-pass filters which prevent WAC control to work in steady-state and to eliminate interactions with non-modeled high-frequency modes [1], [23]. The time-delay and pre-filter transfer function (one for each control signal) can be written in a state-space form as [48]

$$\dot{\mathbf{x}}_d = \mathbf{A}_d\mathbf{x}_d + \mathbf{B}_d\mathbf{v} \tag{3}$$

$$\mathbf{u} = \mathbf{C}_d\mathbf{x}_d + \mathbf{D}_d\mathbf{v} \tag{4}$$

where $\mathbf{v}$ are the control signals at the central station, and $\mathbf{u}$ are the control signals which arrive at the local controllers after the transmission time delay. A dynamic extension to include this time-delay model in the controller design was accomplished by joining the reduced model (1) and (2) with the time-delay model (3) and (4), yielding

$$\dot{\mathbf{x}}_e = \begin{bmatrix} \mathbf{A}_r & \mathbf{B}_r\mathbf{C}_d \\ \mathbf{0} & \mathbf{A}_d \end{bmatrix}\mathbf{x}_e + \begin{bmatrix} \mathbf{B}_r\mathbf{D}_d \\ \mathbf{B}_d \end{bmatrix}\mathbf{v} \tag{5}$$

$$\mathbf{y} = [\,\mathbf{C}_r \quad \mathbf{0}\,]\mathbf{x}_e \tag{6}$$

where $\mathbf{x}_e \triangleq [\mathbf{x}_r\ \mathbf{x}_d]^T$ is an extended state vector to be fed back.

C. Control Law Design Using the State-Space Approach

A MIMO state-feedback scheme was chosen to design the WAC controller because it allows an easier control tuning and higher performance when several measurement channels and control of multiple devices are involved. To control the system (5), the input vector $\mathbf{v}$ was implemented as follows:

$$\mathbf{v} = -\mathbf{K}\mathbf{x}_e = -\mathbf{K}[\mathbf{x}_r\ \mathbf{x}_d]^T. \tag{7}$$

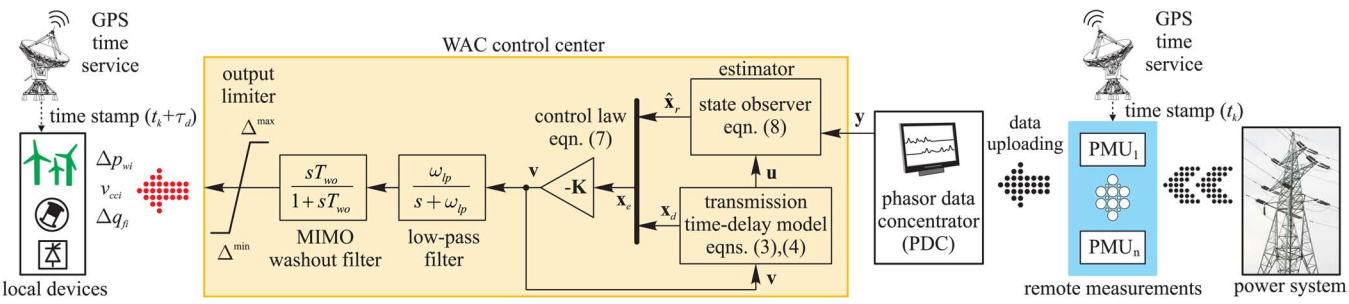

Fig. 3. Block diagram showing the implementation of the proposed wide-area POD control.

The control gain $\mathbf{K}$ was calculated based on an optimal quadratic technique (LQR) to achieve a high oscillation damping and minimize the control efforts. The optimal gain $\mathbf{K}$ was obtained by minimizing the cost function $J = \int(\mathbf{y}^T\mathbf{Q}\mathbf{y} + \mathbf{v}^T\mathbf{R}\mathbf{v})dt$, where $\mathbf{Q}$ is the weighting matrix of the outputs $\mathbf{y}$, and $\mathbf{R}$ is the weighting matrix of the control signals $\mathbf{v}$. A larger value in the diagonal of $\mathbf{R}$, will penalize more the corresponding control input, and a smaller control energy will be spent for this actuator. On the other hand, to make transient angle variations go to zero more quickly, a larger value must be set in the corresponding row of $\mathbf{Q}$ [48].

The controller output was also limited to prevent excessive control action after a large system disturbance.

D. Estimation of the Reduced States

Although the reduced system behaves like the original one, from an input–output point of view ($\mathbf{u} \mapsto \mathbf{y}$), the reduced states $\mathbf{x}_r$ do not have physical meaning and cannot be measured. Reduction methods are useful to design input-output controllers like PSSs or lead-lag compensators; however, to design a MIMO state-feedback controller, some issues must be considered. The internal states $\mathbf{x}_r$ can be estimated from the measures $\mathbf{y}$ using the system (1) and (2), by means of a state observer (software sensor) [48] as follows:

$$\dot{\hat{\mathbf{x}}}_r = \mathbf{A}_r\hat{\mathbf{x}}_r + \mathbf{B}_r\mathbf{u} + \mathbf{G}(\mathbf{y} - \mathbf{C}_r\hat{\mathbf{x}}_r) \tag{8}$$

where $\hat{\mathbf{x}}_r$ are the estimated states of the reduced model. To find the gain matrix $\mathbf{G}$, we defined the estimation error as $\mathbf{e} \triangleq \mathbf{x}_r - \hat{\mathbf{x}}_r$, then the estimation error dynamics was obtained by subtracting (8) from (1); consequently, $\dot{\mathbf{e}} = (\mathbf{A}_r - \mathbf{G}\mathbf{C}_r)\mathbf{e}$. Finally, the matrix $\mathbf{G}$ can be designed using the Kalman filter approach, eigenvalue placement, or optimal quadratic regulation; the latter was used in our design [48]. Thereby, the matrix $(\mathbf{A}_r - \mathbf{G}\mathbf{C}_r)$ presents stable eigenvalues, and the estimation error converges to zero with a desired rate.

Fig. 3 shows a block diagram with the implementation of the proposed control. The wide-area POD controller works when relative angle deviations are detected, and, under normal operating conditions, wind farms and other devices accomplish their typical tasks: voltage control and MPP tracking, for example.

V. Performance Testing

The following parameters were considered in the wide-area POD controller design: washout time constant $T_{\mathrm{wo}} = 5$ s, low-pass filter frequency $\omega_{lp} = 2\pi \times 3.5$ Hz, and reduced-model order $n_r = 30$. The control and observer optimal quadratic gains $\mathbf{K}$ and $\mathbf{G}$ were computed by solving the associated algebraic Riccati equation (ARE) [48] using the design matrices $\mathbf{Q} = \mathbf{I}^{6\times6}$ and $\mathbf{R} = \mathrm{diag}([24\mathbf{I}^{3\times3}\ 0.016\mathbf{I}^{7\times7}])$ for the control law, and $\mathbf{Q} = 500\mathbf{I}^{n_r\times n_r}$ and $\mathbf{R} = \mathbf{I}^{6\times6}$ for the observer. A slope of 5% was chosen in the voltage droop controls and short-term frequency regulation of WECS. The total time delay associated with the PMUs and communication channels (due to transducers, processing time of the phase detection algorithm, link propagation delay, and data concentrators) is modeled as a time delay of $\tau_d = 500$ ms [49]. In the time-domain model of the system, this is represented using a third-order Padé approximation.

Four control cases were evaluated and compared. First, only classical local controllers were considered (Base case). Second, local controllers were also considered, but the short-term frequency regulation in WECS was activated (SFR-Base case). Third, local controllers and POD control coordinating only SGs and FACTS were implemented (C-WAC case). Finally, full hierarchical control was considered including wind farms along with SGs and FACTS in the wide-area coordinating control (WF-WAC case).

A. Small-Signal Stability Analysis

Eigenvalues of Base, SFR-Base and C-WAC cases are shown in Fig. 4(a). In the Base case, the poorly damped critical mode at 0.45 Hz (damping ratio of 0.9%) is observed. When the short-term frequency regulation was activated in all wind farms (SFR-Base case), the critical mode increased its damping to 5%, and the damping ratio of the remaining modes was not significantly affected (compare asterisk with diamond markers). This is an important feature because short-term frequency regulation is added to improve the system inertial response, and we have to corroborate that this supplementary control does not interact negatively with system modes. When the C-WAC case controller was considered, there was an improvement in the damping of the critical mode and other higher frequency modes (compare asterisk with circle markers). This improvement highlights the advantage of using remote measurements when low-frequency inter-area modes need to be damped.

To show the benefits of including WECS in wide-area POD controllers, we plotted the C-WAC and WF-WAC cases in Fig. 4(b). When WECS were coordinated in the centralized control, most of the electromechanical modes increased even more their damping ratio, particularly the critical mode, which

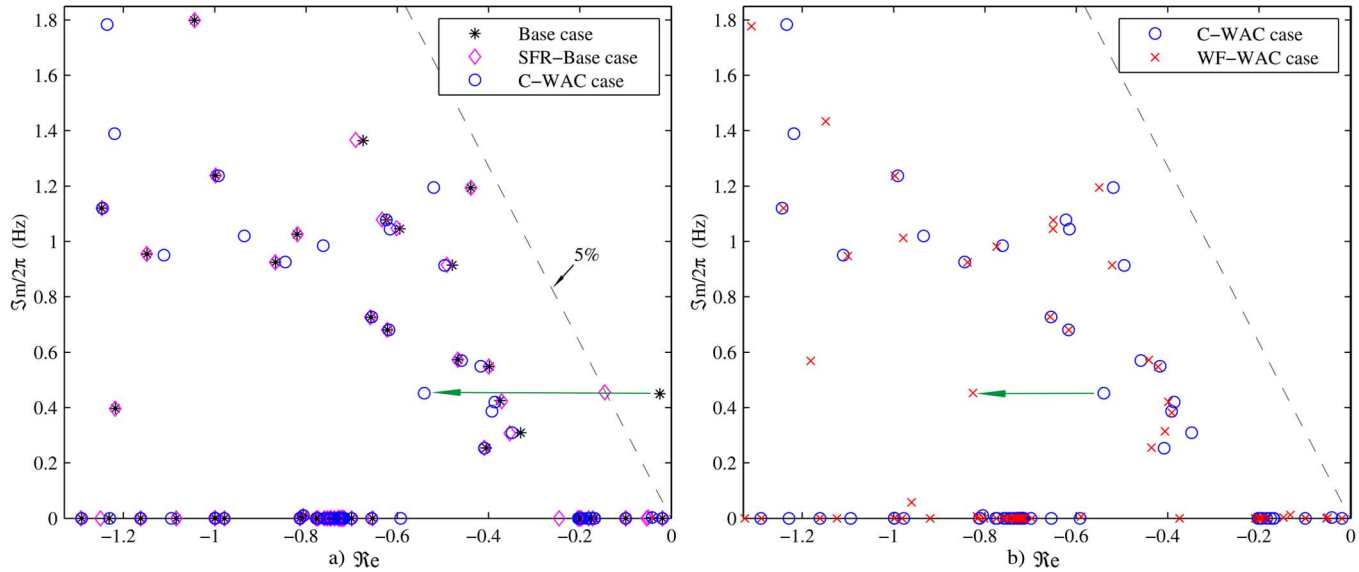

Fig. 4. Eigenvalue comparison for the considered control strategies at the nominal operating condition. (a) Base case (asterisk markers), SFR-Base case (diamond markers), and C-WAC case (circle markers). (b) C-WAC case (circle markers) versus WF-WAC case (cross markers).

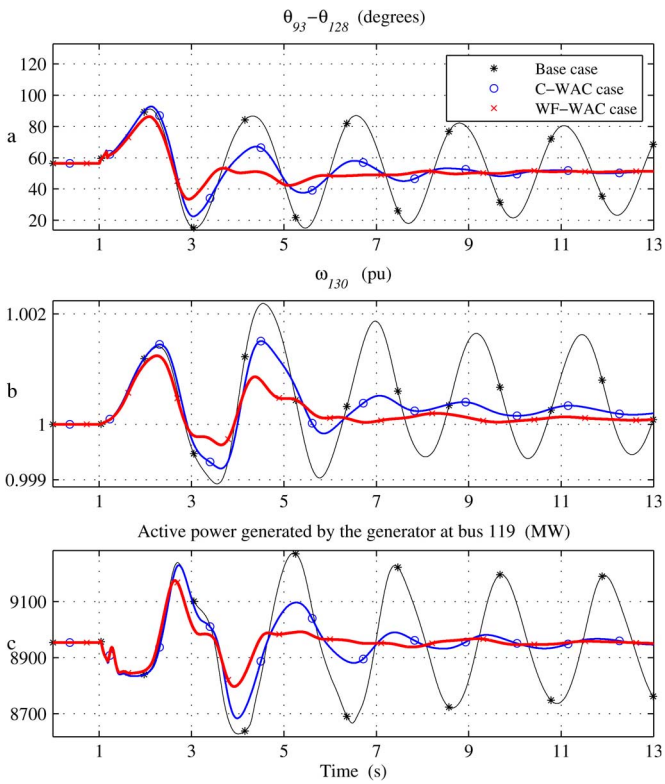

Fig. 5. System transient response against a 150-ms three-phase fault at bus 7. Comparison among Base, C-WAC, and WF-WAC cases: (a) voltage angle difference between buses 93 and 128, (b) rotor speed of generator at bus 130, and (c) active power of generator at bus 119.

increased its damping from 17% to 28% (compare circle with cross markers).

B. Large-Signal Stability Analysis

For the assessment of the performance of the different control cases, we applied a three-phase fault at bus 7, cleared by opening the line between buses 6 and 7. Fig. 5 presents various transient responses for the Base, C-WAC, and WF-WAC cases showing, from an oscillation damping point of view, an agreement with the eigenvalue results obtained at the previous Subsection. The improvements of including multiple WECS in the wide-area POD control, considering both transient excursions and oscillation damping, are seen when comparing the C-WAC and WF-WAC cases. As a result, power system transfer capability can be increased.

To evaluate the impact of the POD controller on wind farms, we showed the injected active power, mechanical speed, and dc-link voltage regulation of the five WECS affected by the WAC control [see Fig. 6(a)-(c)]. The output power is bounded by the limiter, and the MPPT algorithm is reaching the optimal speed after the transient event. The supplementary WAC signals for the three SGs and the two HVDC converter stations are presented, for both the C-WAC and WF-WAC cases, in Fig. 6(d) and (e). In the WF-WAC case, in addition to the oscillation damping increase, the WAC control actions are distributed, and the amplitude of the supplementary remote control signals for the SGs and HVDC stations are smaller, reducing their control efforts. The control efforts of the different devices can be easily weighted by the control design matrix $\mathbf{R}$.

Another test was considered, applying a three-phase fault at bus 2, cleared by opening the line 2–6. Fig. 7 shows the load angles and speed deviations of all synchronous generators. Three cases were analyzed: the Base case, the WF-WAC case without time-delay compensation, and the WF-WAC case with time-delay compensation. In the Base case, growing LFOs arise after the fault and the resulting change in the network topology [see Fig. 7(a) and (b)]. Fig. 7(c) and (d) shows the relevance to take into account the transmission time delay and its proper compensation to avoid deteriorating the system damping even more. On the other hand, there is a highly damped response when the WF-WAC case with time-delay compensation is implemented [see Fig. 7(e) and (f)].

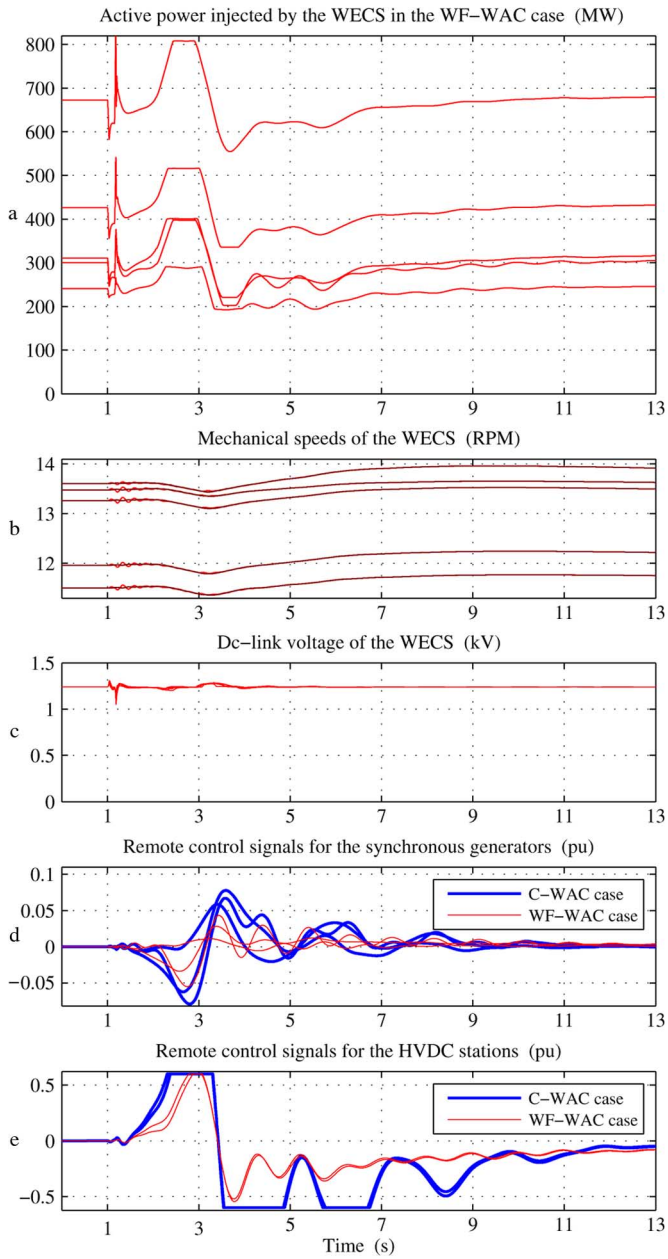

Fig. 6. Transient behavior of the main WECS variables and remote control signals for the SGs and HVDC stations.

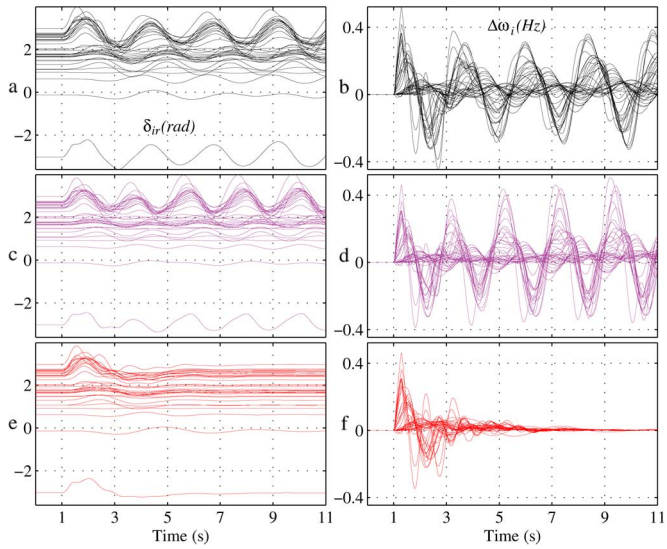

Fig. 7. Transient response of load angles and speed deviations against a fault at bus 2. (a), (b) Base case, (c), (d) WF-WAC case without time-delay compensation, and (d), (e) WF-WAC case with time-delay compensation.

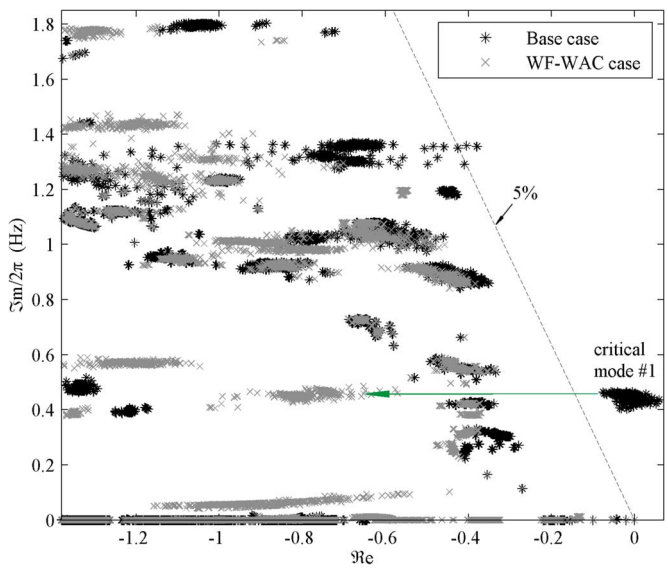

Fig. 8. Closed-loop poles of Base case (dark asterisk markers) and WF-WAC case (light cross markers) for all operating conditions.

C. Robustness Assessment

To analyze the robustness of the proposed POD controller, we considered line outages on the major system ac ties: lines 1–6, 2–6, 6–7, 6–12, 12–25, and 25–27 (other line outages were also studied, but they presented a lower impact on the system dynamics). For each of the above scenarios, we created hundreds of distinct operating points by varying ±30% the dispatched power in all generating stations (these scenarios totaling 686 separate operating conditions). For all of these operating conditions, we implemented the controllers of both the Base case and the WF-WAC case, tuned at the nominal operating scenario. The resulting eigenvalues are shown in Fig. 8 (similar robustness analyses were also carried out in [14], [21], [25]). It was found that the proposed controller significantly damps the critical inter-area mode under different operating conditions. In addition, none of the other modes are adversely impacted; moreover, most of them improve their damping ratio. Other scenarios considering different types of load models, power demand levels, and time-delay uncertainties were analyzed, obtaining similar conclusions (not included due to space limitations).

The robust performance is attained for continuous changes in the electrical network, such as $N-1$ contingencies, daily generation re-dispatch or shedding, which do not considerably modify the locations of the main eigenvalues. However, if substantial transmission network infrastructure is built or new load/generation areas are developed, then the WAC control should be re-tuned to properly perform.

VI. Conclusion

The coordinated control of variable-speed wind power plants with wide-area POD controllers was studied. Several issues were discussed, such as: 1) small- and large-signal perturbation analysis; 2) control design guidelines; 3) robustness assessment; 4) comparison with other classical control strategies; and 5) impact of the supplementary control actions on both power system modes and internal wind farm variables. The proposed POD controller was designed using an observer-based state-feedback approach with transmission time-delay compensation, which allows an easy implementation on large-scale power systems and avoids complex control designs and optimization schemes with high computational cost.

Eigenvalue analyses and nonlinear time-domain simulations on the IEEE 50-machine 145-bus test system were introduced to validate and describe the control methodology. It was found that the coordinated inclusion of multiple wind farms in wide-area controllers can play an effective role to damp inter-area oscillations, with several advantages to the system operation, namely: 1) relaxation of stability constraints; 2) suppression of low-frequency oscillations increasing power transfer capability between interacting areas; and 3) enhanced secure power flows reducing unplanned system separation or blackouts.

To show the satisfactory performance and practical applicability over a wide range of operating points, a robustness assessment was also performed at different operating scenarios such as line outage contingencies, load/generation shedding, and line faults. The obtained results show that encouraging system improvements can be obtained when multiple wind farms are properly added to centralized POD controls using wide-area measurement systems.

Acknowledgment

A. E. Leon would like to thank N. Kirchner and C. Fernández de Kirchner for the political decisions and financial support that made this work possible.

References

[1] J. Chow, J. Sanchez-Gasca, H. Ren, and S. Wang, "Power system damping controller design-using multiple input signals," *IEEE Control Syst. Mag.*, vol. 20, pp. 82–90, Aug. 2000.

[2] M. Aboul-Ela, A. Sallam, J. McCalley, and A. Fouad, "Damping controller design for power system oscillations using global signals," *IEEE Trans. Power Syst.*, vol. 11, no. 2, pp. 767–773, May 1996.

[3] I. Kamwa, R. Grondin, and Y. Hebert, "Wide-area measurement based stabilizing control of large power systems—A decentralized/hierarchical approach," *IEEE Trans. Power Syst.*, vol. 16, no. 1, pp. 136–153, Feb. 2001.

[4] Y. Zhang and A. Bose, "Design of wide-area damping controllers for interarea oscillations," *IEEE Trans. Power Syst.*, vol. 23, no. 3, pp. 1136–1143, Aug. 2008.

[5] F. M. Hughes, O. Anaya-Lara, N. Jenkins, and G. Strbac, "Control of DFIG-based wind generation for power network support," *IEEE Trans. Power Syst.*, vol. 20, no. 4, pp. 1958–1966, Nov. 2005.

[6] J. Mauricio, A. Marano, A. Gomez-Exposito, and J. Martinez Ramos, "Frequency regulation contribution through variable-speed wind energy conversion systems," *IEEE Trans. Power Syst.*, vol. 24, no. 1, pp. 173–180, Feb. 2009.

[7] A. E. Leon, J. M. Mauricio, A. Gomez-Exposito, and J. A. Solsona, "An improved control strategy for hybrid wind farms," *IEEE Trans. Sustain. Energy*, vol. 1, no. 4, pp. 131–141, Oct. 2010.

[8] C. Taylor, D. Erickson, K. Martin, R. Wilson, and V. Venkatasubramanian, "WACS-Wide-area stability and voltage control system: R&D and online demonstration," *Proc. IEEE*, vol. 93, no. 5, pp. 892–906, May 2005.

[9] W. Yao, L. Jiang, Q. Wu, J. Wen, and S. Cheng, "Delay-dependent stability analysis of the power system with a wide-area damping controller embedded," *IEEE Trans. Power Syst.*, vol. 26, no. 1, pp. 233–240, Feb. 2011.

[10] T. Zabaiou, L.-A. Dessaint, F.-A. Okou, and R. Grondin, "Wide-area coordinating control of SVCs and synchronous generators with signal transmission delay compensation," in *Proc. IEEE Power Energy Soc. Gen. Meeting*, Jul. 2010, pp. 1–9.

[11] B. Chaudhuri, R. Majumder, and B. Pal, "Wide-area measurement-based stabilizing control of power system considering signal transmission delay," *IEEE Trans. Power Syst.*, vol. 19, no. 4, pp. 1971–1979, Nov. 2004.

[12] H. Wu, K. Tsakalis, and G. Heydt, "Evaluation of time delay effects to wide-area power system stabilizer design," *IEEE Trans. Power Syst.*, vol. 19, no. 4, pp. 1935–1941, Nov. 2004.

[13] N. Chaudhuri, S. Ray, R. Majumder, and B. Chaudhuri, "A new approach to continuous latency compensation with adaptive phasor power oscillation damping controller (POD)," *IEEE Trans. Power Syst.*, vol. 25, no. 2, pp. 939–946, May 2010.

[14] R. Preece, J. Milanovic, A. Almutairi, and O. Marjanovic, "Probabilistic evaluation of damping controller in networks with multiple VSC-HVDC lines," *IEEE Trans. Power Syst.*, vol. 28, no. 1, pp. 367–376, Feb. 2013.

[15] R. Shah, N. Mithulananthan, and K. Lee, "Large-scale PV plant with a robust controller considering power oscillation damping," *IEEE Trans. Energy Convers.*, vol. 28, no. 1, pp. 106–116, Jan. 2013.

[16] D. P. Ke, C. Chung, and Y. Xue, "An eigenstructure-based performance index and its application to control design for damping inter-area oscillations in power systems," *IEEE Trans. Power Syst.*, vol. 26, no. 4, pp. 2371–2380, Nov. 2011.

[17] D. Dotta, A. e Silva, and I. Decker, "Wide-area measurements-based two-level control design considering signal transmission delay," *IEEE Trans. Power Syst.*, vol. 24, no. 1, pp. 208–216, Feb. 2009.

[18] P. Zhang, D. Yang, K. Chan, and G. Cai, "Adaptive wide-area damping control scheme with stochastic subspace identification and signal time delay compensation," *IET Gener., Transm. Distrib.*, vol. 6, no. 9, pp. 844–852, 2012.

[19] J. Milanovic and A. Duque, "Identification of electromechanical modes and placement of PSSs using relative gain array," *IEEE Trans. Power Syst.*, vol. 19, no. 1, pp. 410–417, Feb., 2004.

[20] Y. Li, C. Rehtanz, S. Ruberg, L. Luo, and Y. Cao, "Wide-area robust coordination approach of HVDC and FACTS controllers for damping multiple interarea oscillations," *IEEE Trans. Power Del.*, vol. 27, no. 3, pp. 1096–1105, Mar. 2012.

[21] L. Kunjumuhammed, R. Singh, and B. Pal, "Robust signal selection for damping of inter-area oscillations," *IET Gener., Transm. Distrib.*, vol. 6, no. 5, pp. 404–416, 2012.

[22] Y. Pipelzadeh, B. Chaudhuri, and T. Green, "Wide-area power oscillation damping control through HVDC: A case study on Australian equivalent system," in *Proc. IEEE Power Energy Soc. Meeting*, 2010, pp. 1–7.

[23] Y. Li, C. Rehtanz, D. Yang, S. Ruberg, and U. Hager, "Robust high-voltage direct current stabilising control using wide-area measurement and taking transmission time delay into consideration," *IET Gener., Transm. Distrib.*, vol. 5, no. 3, pp. 289–297, 2011.

[24] J. Sanchez-Gasca and J. Chow, "Power system reduction to simplify the design of damping controllers for interarea oscillations," *IEEE Trans. Power Syst.*, vol. 11, no. 3, pp. 1342–1349, Aug. 1996.

[25] A. Zolotas, B. Chaudhuri, I. Jaimoukha, and P. Korba, "A study on LQG/LTR control for damping inter-area oscillations in power systems," *IEEE Trans. Control Syst. Technol.*, vol. 15, no. 1, pp. 151–160, Jan. 2007.

[26] R. Preece, J. Milanovic, A. Almutairi, and O. Marjanovic, "Damping of inter-area oscillations in mixed AC/DC networks using WAMS based supplementary controller," *IEEE Trans. Power Syst.*, vol. 28, no. 2, pp. 1160–1169, May 2013.

[27] S. Azad, R. Iravani, and J. Tate, "Damping inter-area oscillations based on a model predictive control (MPC) HVDC supplementary controller," *IEEE Trans. Power Syst.*, vol. 28, no. 3, pp. 3174–3183, Aug. 2013.

[28] M. Mokhtari, F. Aminifar, D. Nazarpour, and S. Golshannavaz, "Wide-area power oscillation damping with a fuzzy controller compensating the continuous communication delays," *IEEE Trans. Power Syst.*, vol. 28, no. 2, pp. 1997–2005, May 2013.
[29] H. Huang and C. Chung, "Coordinated damping control design for DFIG-based wind generation considering power output variation," *IEEE Trans. Power Syst.*, vol. 27, no. 4, pp. 1916–1925, Nov. 2012.
[30] N. D. Caliao, G. Ramtharan, J. Ekanayake, and N. Jenkins, "Power oscillation damping controller for fully rated converter wind turbines," in *Proc. Int. Univer. Power Eng. Conf.*, 2010, pp. 1–6.
[31] T. Knuppel, J. Nielsen, K. Jensen, A. Dixon, and J. Ostergaard, "Power oscillation damping capabilities of wind power plant with full converter wind turbines considering its distributed and modular characteristics," *IET Renew. Power Gener.*, vol. 7, no. 5, pp. 431–442, 2013.
[32] L. Fan, H. Yin, and Z. Miao, "On active/reactive power modulation of DFIG-based wind generation for interarea oscillation damping," *IEEE Trans. Energy Convers.*, vol. 26, no. 2, pp. 513–521, Jun. 2011.
[33] A. Adamczyk, R. Teodorescu, and P. Rodriguez, "Control of full-scale converter based wind power plants for damping of low frequency system oscillations," in *Proc. IEEE Trondheim PowerTech*, 2011, pp. 1–7.
[34] W. Qiao, G. Venayagamoorthy, and R. Harley, "DHP-based wide-area coordinating control of a power system with a large wind farm and multiple FACTS devices," in *Proc. Int. Joint Conf. Neural Networks*, 2007, pp. 2093–2098.
[35] A. E. Leon, J. M. Mauricio, A. Gomez-Exposito, and J. A. Solsona, "Hierarchical wide-area control of power systems including wind farms and FACTS for short-term frequency regulation," *IEEE Trans. Power Syst.*, vol. 27, no. 4, pp. 2084–2092, Nov. 2012.
[36] A. E. Leon, J. M. Mauricio, and J. A. Solsona, "Fault ride-through enhancement of DFIG-based wind generation considering unbalanced and distorted conditions," *IEEE Trans. Energy Convers.*, vol. 27, no. 3, pp. 775–783, Sep. 2012.
[37] P. Kundur, *Power System Stability and Control*. New York, NY, USA: McGraw-Hill, 1994.
[38] V. Akhmatov and H. Knudsen, "An aggregate model of a grid-connected, large-scale, offshore wind farm for power stability investigations-Importance of windmill mechanical system," *Int. J Electr. Power Energ Syst.*, vol. 24, no. 9, pp. 709–717, 2002.
[39] S. Muyeen, M. Ali, R. Takahashi, T. Murata, J. Tamura, Y. Tomaki, A. Sakahara, and E. Sasano, "Comparative study on transient stability analysis of wind turbine generator system using different drive train models," *IET Renew. Power Gener.*, vol. 1, pp. 131–141, Jun. 2007.
[40] J. Slootweg, S. de Haan, H. Polinder, and W. Kling, "General model for representing variable speed wind turbines in power system dynamics simulations," *IEEE Trans. Power Syst.*, vol. 18, no. 1, pp. 144–151, Feb. 2003.
[41] M. Tsili and S. Papathanassiou, "A review of grid code technical requirements for wind farms," *IET Renew. Power Gener.*, vol. 3, pp. 308–332, Sep. 2009.
[42] A. E. Leon and J. A. Solsona, "Performance improvement of full-converter wind turbines under distorted conditions," *IEEE Trans. Sustain. Energy*, vol. 4, no. 3, pp. 652–660, Jul. 2013.
[43] R. Eriksson and L. Soder, "Wide-area measurement system-based subspace identification for obtaining linear models to centrally coordinate controllable devices," *IEEE Trans. Power Del.*, vol. 26, no. 4, pp. 988–997, Apr. 2011.
[44] Y. Li, C. Rehtanz, S. Ruberg, L. Luo, and Y. Cao, "Assessment and choice of input signals for multiple HVDC and FACTS wide-area damping controllers," *IEEE Trans. Power Syst.*, vol. 27, no. 4, pp. 1969–1977, Nov. 2012.
[45] Y. Pipelzadeh, N. Chaudhuri, B. Chaudhuri, and T. C. Green, "System stability improvement through optimal control allocation in voltage source converter-based high-voltage direct current links," *IET Gener., Transm. Distrib.*, vol. 6, no. 9, pp. 811–821, 2012.
[46] M. Farsangi, Y. H. Song, and K. Lee, "Choice of FACTS device control inputs for damping interarea oscillations," *IEEE Trans. Power Syst.*, vol. 19, no. 2, pp. 1135–1143, May 2004.
[47] M. Safonov and R. Chiang, "A schur method for balanced-truncation model reduction," *IEEE Trans. Autom. Control*, vol. 34, no. 7, pp. 729–733, Jul. 1989.
[48] K. Ogata, *Modern Control Engineering*. Upper Saddle River, NJ, USA: Prentice-Hall, 1997.
[49] B. Naduvathuparambil, M. Valenti, and A. Feliachi, "Communication delays in wide area measurement systems," in *Proc. 34th Southeastern Symp. Syst. Theory*, 2002, pp. 118–122.

Andres E. Leon (S'05–M'13) was born in Argentina in 1979. He received the Electrical Engineering degree from Universidad Nacional del Comahue, Neuquén, Argentina, in 2005, and the Ph.D. degree from Universidad Nacional del Sur, Bahía Blanca, Argentina, in 2011.

Since 2012, he has been an Assistant Researcher with the National Scientific and Technical Research Council (CONICET), developing his work at the Research Institute of Electrical Engineering (Instituto de Investigaciones en Ingeniería Eléctrica "Alfredo Desages", IIIE), Bahía Blanca, Argentina. His primary areas of interest are power system control and wind energy conversion systems.

Jorge A. Solsona (SM'04) received the Electronics Engineer and Ph.D. degrees from the Universidad Nacional de La Plata, La Plata, Argentina, in 1986 and 1995, respectively.

Currently, he is with the Instituto de Investigaciones en Ingeniería Eléctrica Alfredo Desages (IIIE), Departamento de Ingeniería Eléctrica y de Computadoras, Universidad Nacional del Sur, Bahía Blanca, Argentina, and CONICET, where he is involved in teaching and research on control theory and its applications to electromechanical systems.